

Fatty Acid Amide Hydrolase Inhibitors from Virtual Screening of the Endocannabinoid System

Susanna M. Saario,^{*,†} Antti Poso,[†] Risto O. Juvonen,[‡] Tomi Järvinen,[†] and Outi M. H. Salo-Ahen[†]

Department of Pharmaceutical Chemistry and Department of Pharmacology and Toxicology, University of Kuopio, P.O. Box 1627, FIN-70211 Kuopio, Finland

Received April 4, 2006

The endocannabinoid system consists of two cannabinoid receptors (CB1 and CB2), endogenous ligands (endocannabinoids), and the enzymes involved in the metabolism of the endocannabinoids, including fatty acid amide hydrolase (FAAH) and monoglyceride lipase (MGL). In the present study, virtual screening of MGL inhibitors was performed by utilizing a comparative model of the human MGL enzyme. All hit molecules were tested for their potential MGL inhibitory activity, but no compounds were found capable of inhibiting MGL-like enzymatic activity in rat cerebellar membranes. However, these compounds were also tested for their potential FAAH inhibitory activity and five compounds (2–6) inhibiting FAAH were found with IC_{50} values between 4 and 44 μM . In addition, the hit molecules from the virtual screening of CB2 receptor ligands (reported previously in Salo et al. *J. Med. Chem.* 2005, 48, 7166) were also tested in our FAAH assay, and four active compounds (7–10) were found with IC_{50} values between 0.52 and 22 μM . Additionally, compound 7 inhibited MGL-like enzymatic activity with an IC_{50} value of 31 μM .

Introduction

N-Arachidonylethanolamide (AEA) and 2-arachidonoylglycerol (2-AG, **1**; Figure 1) are the most abundant endogenous ligands for the G-protein-coupled central CB1 and peripheral CB2 cannabinoid receptors.^{1–3} The endocannabinoids are produced by neurons on demand and act near to the site of their synthesis, and, as is typical of neuromodulators, they are effectively metabolized to ensure rapid signal inactivation.^{1–3} The enzymatic hydrolysis of AEA to arachidonic acid and ethanolamine is catalyzed by fatty acid amide hydrolase (FAAH),^{4–7} whereas the hydrolysis of **1** has previously been reported to be catalyzed by monoglyceride lipase (MGL; EC 3.1.1.23).⁸ FAAH has a broad amide substrate specificity, and despite its name, this enzyme is also able to catalyze the hydrolysis of fatty acid esters, including **1**.⁹ MGL is a serine hydrolase that hydrolyses 2- and 1(3)-ester bonds of monoglycerides to fatty acid and glycerol.¹⁰ Unlike FAAH, MGL does not recognize fatty acid amides as substrates.

FAAH has previously been reported to be a potential therapeutic target for the treatment of inflammatory pain and anxiety.^{11,12} A number of potent FAAH inhibitors have been reported, including the nonselective methyl arachidonyl fluorophosphonate (MAFP)¹³ and hexadecylsulfonyl fluoride (HDSF),¹⁴ and the selective URB597,¹² OL-53,¹⁵ and OL-135.¹⁶ With respect to MGL, only a few inhibitors have been reported to date. Recently, Makara et al. (2005) reported that URB754 was a selective MGL inhibitor with an IC_{50} value of 200 nM.¹⁷ In our previous study we reported that a maleimide compound with an arachidonic moiety (*N*-arachidonyl maleimide; NAM) inhibited MGL-like enzymatic activity in rat cerebellar membranes with an IC_{50} value of 140 nM.¹⁸ True MGL activity, as well as MGL-like activity in our test system, can also be inhibited by several serine hydrolase inhibitors such as MAFP and HDSF.^{19,20}

Inhibition of the endocannabinoid hydrolases could offer a rational therapeutic approach in treating certain disease states,

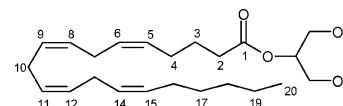


Figure 1. Chemical structure of **1**.

such as anxiety and inflammatory pain, in which a higher endocannabinoid activity would be beneficial. One advantage of this kind of enzyme inhibition over direct cannabinoid agonists could be higher selectivity, as the intervention would increase the activity of the endocannabinoid system only at the sites where the endocannabinoids are produced. This hypothesis has been supported by animal studies in which the FAAH inhibitor URB597 elevated endocannabinoid tone and, unlike the nonselective cannabinoid agonists, did not produce any motor side effects, such as catalepsy.^{11,12} In the present study, a comparative model of the human MGL enzyme was utilized for the virtual screening of novel MGL inhibitors. Since most of the current MGL inhibitors are nonselective and usually inhibit also FAAH, all hit molecules were tested in our MGL and FAAH assays for their potential inhibitory activity. Additionally, since many of the cannabinergic molecules can act on more than one of the endocannabinoid target proteins (CB1, CB2, MGL, FAAH, or the putative AEA transporter AMT), the hit molecules obtained from the virtual screening of CB2 ligands reported in our previous study²¹ were also tested in our MGL and FAAH assays.

Results and Discussion

Molecular Modeling of Human MGL Enzyme. As described in the Experimental Section, the comparative model for hMGL was constructed in an analogous way with the previously reported rat MGL model.¹⁸ Since the hMGL sequence is 83.8% identical with the rat MGL and the sequences are of similar length (303 residues), there were no significant differences between the models. The MD simulation results of the modeled structure were comparable with those attained with the chloroperoxidase L crystal structure (see Supporting Information, sections D–F); the simulations were energetically stable and the protein secondary structures were well conserved; the rmsd deviation of the protein backbone from the initial structures rose

* To whom correspondence should be addressed: Tel: +358-17-163713. Fax: +358-17-162456. E-mail: susanna.saario@uku.fi.

[†] Department of Pharmaceutical Chemistry.

[‡] Department of Pharmacology and Toxicology.

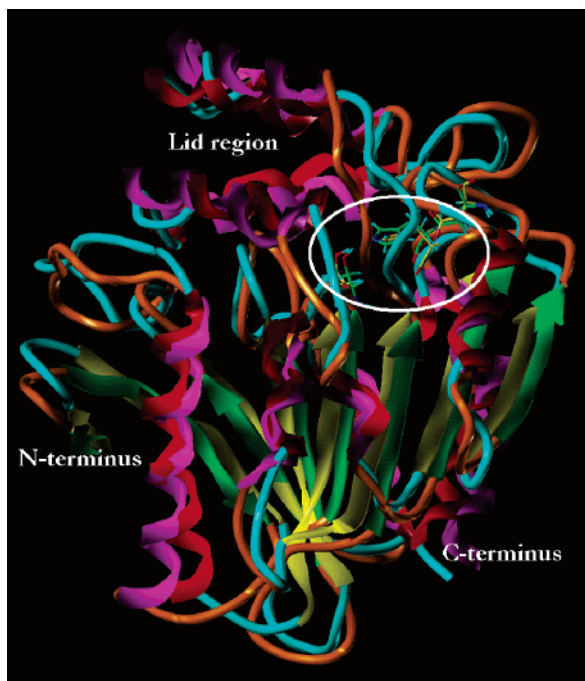


Figure 2. Human MGL model before and after the 2370-ps MD simulation. Secondary structure coding: α helix, magenta (before MD)/red (after MD); β sheet, green (before MD)/yellow (after MD); other, orange (before MD)/cyan (after MD). Catalytic triad is circled by the ellipse; residue color code: carbon, green (before MD)/yellow (after MD); nitrogen, blue; oxygen, red; hydrogen, cyan.

to ca. 2 Å for the template and to 2.3 Å for the hMGL model. Most of the movement was due to the flexible loops in the 'lid' region, whereas the core β sheet was the most stable (Figure 2). The PROCHECK²² analysis indicated that the energy-minimized final frame structures of the template and the model had comparable stereochemistry (Supporting Information, section G).

Database Searches. The MGL substrate **1** was docked into the hMGL model and used for defining both the UNITY²³ and BRUTUS^{24,25} database searches. The conformer of **1** that was chosen for the queries had the following distances to the residues important for the catalysis reaction: from carbonyl oxygen of **1** to backbone NH hydrogen of Ala51, 2.97 Å; from carbonyl oxygen of **1** to backbone NH nitrogen of Met123, 2.60 Å; from carbonyl carbon of **1** to hydroxyl oxygen of Ser122, 2.56 Å. The hydrophobic tail of the docked substrate was directed up to the 'lid' region of the enzyme model. The conformer chosen for **7** in BRUTUS search was fitted into the binding cavity in a similar curved conformation as **1**; the five-membered heteroring of **7** reached to the C14 of **1**, the aromatic ring of **7** was aligned with the C8–C9 double bond of **1**, and the *N*-alkyl tail oriented to the same region with the polar headgroup of **1**.

In query 1 (Q1, Figure 3), the query features were taken from both the putative binding site of **1** and the substrate. Q1 was used for searching the LeadQuest compound library,²⁶ and even though this search had to be discontinued, it produced 97 hit molecules. Later, as we analyzed this query, we found that there was a mistake in calculating the MOLCAD²⁷ separated surface for the surface volume constraint (the substrate had been mistakenly included in the 3-Å shell surrounding the docked substrate). With the present version of SYBYL²⁸ (v. 7.1) we could no longer reproduce that surface as the program reported an error message. The erroneous surface constraint resulted in hits that were outside the surface but matched the two donor sites defined by the backbone nitrogens of Gly50 and Met123.

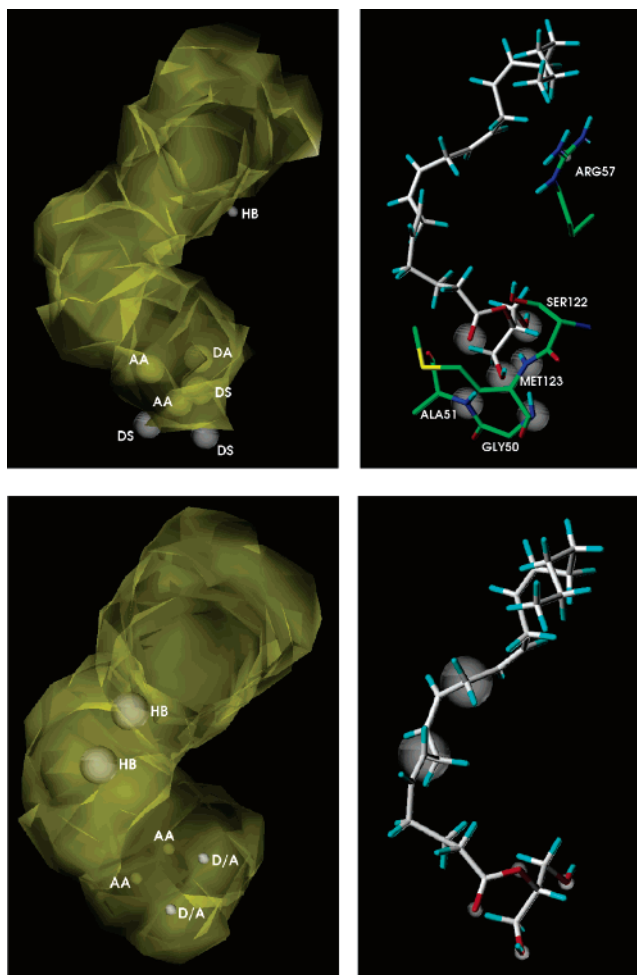


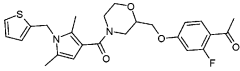
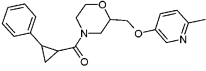
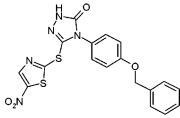
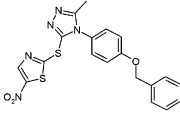
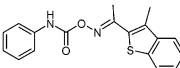
Figure 3. Graphical representations of query 1 (left, top) and query 2 (left, below); feature code: HB, hydrophobic; DA, donor atom; AA, acceptor atom; D/A, donor or acceptor atom; DS, donor site; yellow surface, surface volume constraint. Query 1 without the surface volume constraint (right, top); the docked 2-AG and the residues used for defining the query features are also shown; Query 2 without the surface volume constraint (right, below); the docked 2-AG used for defining the query features is also shown. Color code: gray, ligand carbon; green, protein carbon; red, oxygen; blue, nitrogen; cyan, hydrogen; only the essential hydrogen atoms of the protein residues are shown.

Features for query 2 (Q2, Figure 3) were defined by the docked substrate **1**. Additionally, the surface volume constraint defined by the separated surface between **1** and its binding site (shell 3 Å) was applied. This query produced 1825 hits from the Maybridge²⁹ database and 551 hits from the LeadQuest library.

All these virtual hit molecules were filtered through docking and scoring in the MGL model. Finally, 51 compounds of the best-ranked hit molecules were ordered for in vitro testing of their biological activity. We also ordered 11 molecules chosen from the BRUTUS database search hits.

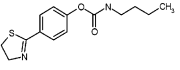
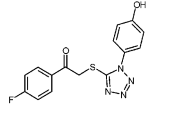
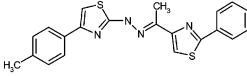
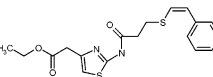
In Vitro Studies. The hit molecules from virtual screening for MGL inhibitors were tested for their ability to inhibit MGL-like activity in rat cerebellar membranes. Unfortunately, no inhibitors of the MGL-like enzyme in rat cerebellar membranes were found. One reason for this failure could be that the enzyme responsible for 2-AG hydrolysis in rat cerebellar membranes is distinct from MGL, as the monoacylglycerols have also been reported to be hydrolyzed by other lipases and esterases.^{30,31} Also, one has to bear in mind that the present MGL model is only a crude estimate of reality.

Table 1. IC₅₀ Values of MGL Hit Molecules for Their Ability to Inhibit FAAH

compound	structure	IC ₅₀ value (95% CI), μM ^a
(2) TRIPOS 676019		8 (6-10)
(3) TRIPOS 673991		44 (33-59)
(4) SPB 07894		4 (3-5)
(5) SPB 07951		32 (23-46)
(6) MWP 00348		4 (3-5)

^a Values represent mean (95% confidence intervals in parentheses) from three independent experiments performed in duplicate.

Table 2. IC₅₀ Values of CB2 Receptor Hit Molecules for Their Ability to Inhibit FAAH

compound	structure	IC ₅₀ value (95% CI), μM ^a
(7) SPB 01403		0.52 (0.39-0.70)
(8) HTS 00798		7 (5-10)
(9) SPB 03742		0.69 (0.53-0.90)
(10) TRIPOS 553110		22 (16 - 30)

^a Values represent mean (95% confidence intervals in parentheses) from three independent experiments performed in duplicate.

In the present study, however, nine novel FAAH inhibitors (2–10) were found from the hits of the MGL and CB2 comparative model-based virtual screening. Due to the nonselectivity of many cannabinergic compounds, it was reasonable to test the virtual screening hits from both of these studies for their FAAH inhibition. For example, compound 1 is an agonist at both the cannabinoid receptors and a substrate for both MGL and FAAH. Consequently, five (2–6) of these nine FAAH inhibitors were found from among the 62 MGL hit molecules to inhibit FAAH in rat brain homogenate with IC₅₀ values between 4 and 44 μM (see Table 1). Compounds 2 and 3 matched the Q1 donor sites (corresponding to the backbone NH groups of Gly50 and Met123) with their acceptor atoms that were separated ca. 4.85 Å from each other (ether and carbonyl oxygen, respectively). Compounds 4 and 5 found by Q2 matched one hydrophobic feature (the one associated with C10 of 1) with their aromatic rings (middle 6-ring) and the two plain acceptor

atom features with their nitro groups. Compound 6 was found with BRUTUS using 7 as the template.

Additionally, four (7–10) of these FAAH inhibitors were found from among the 86 CB2 hit molecules and they inhibited FAAH in rat brain homogenate with IC₅₀ values between 0.52 and 22 μM (see Table 2). Compound 7 inhibited also MGL-like activity in rat cerebellar membranes with an IC₅₀ value of 31 μM (95% confidence interval [CI], 25–39 μM; *n* = 3). Compounds 7–10 did not possess any CB2 receptor activity.²¹

The structures of the nine FAAH inhibitors found in this study do not significantly resemble any previously reported FAAH inhibitors. Compound 7, the most potent FAAH inhibitor (IC₅₀; 520 nM) in this group contains a carbamate carbon which is also present in URB597. URB597 inhibited AEA hydrolysis in our assay with an IC₅₀ value of 3.8 nM (95% CI, 2.9–5.0 nM; *n* = 3), which is comparable to the previously reported IC₅₀ value of 4.6 nM.¹² However, compound 9, which does not

contain a carbamate carbon or even any carbonyl carbon, inhibited FAAH with an almost identical IC_{50} value (690 nM) to that of compound **7**. On the basis of this observation, it may be presumed that a carbonyl carbon is not necessary for inhibiting FAAH.

In our previous study we reported that the maleimide compound, NAM, inhibited MGL-like enzymatic activity in rat cerebellar membranes with an IC_{50} value of 140 nM.¹⁸ In subsequent studies, NAM was found to have 25-fold selectivity toward MGL-like enzyme activity compared to FAAH. NAM inhibited FAAH in rat brain homogenate with an IC_{50} value of 3.3 μ M (95% CI, 2.8–3.8 μ M; $n = 3$).

Docking Studies at the FAAH Crystal Structure. We docked all active FAAH inhibitors found in the present study in the FAAH crystal structure³² (pdb1mt5) to investigate the binding mode and structure–activity relationships of the compounds. Although exact docking modes of the active compounds cannot exclusively be revealed, some trends were clear. In all successful dockings (as judged by the GOLD fitness score and consensus scoring), the ligand had a favorable interaction with at least some of the residues. The most frequent interaction partners were Gly239, Ile238 (hydrogen bond to the backbone amide nitrogens), Met191 (hydrogen bond to the peptide oxygen), and the side-chain oxygens of Ser217 and Ser241. In addition, the protonated nitrogen of Lys142 seemed to be close to almost all ligands. Surprisingly, none of the docked ligands was found within the cavity occupied by the arachidonyl tail of MAFP.

Conclusion

In the present study nine novel FAAH inhibitors (**2–10**) were found from the hits of the MGL and CB2 comparative model-based virtual screening. The most active compound (**7**) in this group inhibited FAAH and MGL-like enzyme activity with IC_{50} values of 520 nM and 31 μ M, respectively. Compound **7** contains a carbamate group which is also present in the potent FAAH inhibitor URB597. However, compound **9** which does not contain any carbonyl carbon inhibited FAAH with an almost identical IC_{50} value (690 nM) to that of compound **7**. This result indicates that a carbonyl group is not essential for inhibiting FAAH. The present hit molecules serve as lead structures for novel FAAH inhibitors that are intended for therapeutic use.

Experimental Section

Molecular Modeling of Human MGL Enzyme. A comparative model of human MGL (hMGL) was constructed employing the same method and template as for the rat MGL model described in our previous study.¹⁸ The hMGL sequence (Q96AA5) was retrieved from the SWISS-PROT/TrEMBL database³³ and the X-ray structure of chloroperoxidase L (EC 1.11.1.10; pdb1a88; chain A)³⁴ from the Protein Data Bank (PDB)³⁵ (see the modeling alignment in Supporting Information, section A). The HOMOLOGY module of the InsightII v.2000 modeling package³⁶ was used in the process of comparative modeling. The coordinates of Gly100 and Gly172 in the chloroperoxidase structure were omitted, and the resulting gaps in the MGL model were repaired by joining the chain ends of the neighboring residues. The resulting enzyme model was subjected to energy minimization by the SYBYL v. 6.9 modeling program³⁷ as follows: (i) 50 iterations (Kollman United force field³⁸) with both the steepest descent method and the conjugate gradient minimizer, keeping the catalytic triad and the backbone atoms of the secondary structures fixed; (ii) 50 iterations with the conjugate gradient minimizer, allowing additionally amino acids 124–127 and 184–187 to move (relaxing the backbone strain caused by coordinate deletions); (iii) 100 iterations (Kollman All-Atom force field³⁹) with the conjugate gradient minimizer, keeping the same

aggregate as in the previous step; (iv) 20 iterations with the conjugate gradient minimizer, keeping only the catalytic triad as an aggregate.

For the purpose of examining the stability of the model, a series of molecular dynamics (MD) simulations was performed on the enzyme structure by using the GROMACS package.^{40,41} The modeled structure was placed in a cubic water box at 300 K. We utilized the SPC⁴² water in the Gromacs^{41,43} force field and added two sodium ions to neutralize the total charge of the system. Particle mesh Ewald (PME)⁴⁴ electrostatics and periodic boundary conditions were used in the simulation, as well as pressure and temperature coupling⁴⁵ to an external bath. A total time span of 2370 ps was simulated. The position restraints on the protein backbone atoms were gradually decreased (initially 1000 kJ/mol \times nm²) so that in the end the whole enzyme structure could move freely for 1500 ps (see Supporting Information, sections B and C for the detailed MD parameters and description of the used constraints). For comparison, similar MD simulations were performed on the chloroperoxidase L crystal structure. After the simulations were completed, the final structures were energy-minimized in SYBYL 6.9 (conjugate gradient minimizer, 25 iterations, Kollman All-Atom force field). Also, the hydroxyl hydrogen of Ser122 at MGL was directed toward the NE2 nitrogen of His269. The stereochemical quality of the resulting protein structures was checked with the PROCHECK program.²²

Molecular Docking of **1.** The MGL substrate **1** was docked at the putative binding site of MGL by the GOLD program⁴⁶ (v. 2.0). The hydroxyl oxygen of the reactive Ser122 was used as a center atom for defining the docking cavity (cavity radius = 15 Å). In addition, a distance constraint of 1.2–2.5 Å was applied between the hydroxyl oxygen of the Ser122 and the carbonyl carbon of **1**. GOLD was allowed to produce 50 different binding conformations/orientations for the ligand. All docking conformations were then relaxed and ranked with CScore,⁴⁷ and conformations with the best scores were checked visually. A conformer of **1** that had reasonable distances to the amino acids important for the catalysis reaction was chosen for the database searches.

UNITY Database Searches. Features from both the modeled enzyme binding site and the docked compound **1** were combined in the first UNITY²³ database query (query 1 = Q1, Figure 3). The carbonyl oxygen and one of the hydroxyl oxygens of **1** were defined as acceptor atoms. The corresponding donor sites on the protein were the backbone nitrogens of Met123 for the carbonyl oxygen and Gly50 and Ala51 for the hydroxyl oxygen. In our MGL model, Ala51 and Met123 are the residues forming the so-called oxyanion hole. These two backbone NH groups are in the proximity of the reactive Ser122 and can donate hydrogen bonds to stabilize the intermediate structure of the reacting substrate during its hydrolysis. In addition, the other hydroxyl group of **1** was defined as a donor atom without a corresponding acceptor site. The tolerance of all the acceptor/donor features was set to 0.75 Å. A hydrophobic feature was placed at the central carbon of the Arg57 guanidinium group (tolerance 0.3 Å), and a plane with a tolerance of 10° was defined by the three nitrogens of this group. A surface volume constraint (tolerance 1.5 Å) was created using a MOLCAD²⁷ separated surface that was calculated between **1** and the enzyme residues within a 3-Å shell around it. Moreover, a partial match constraint was applied on all the acceptor/donor features and the hydrophobic feature so that hit molecules had to match with at least two and at most three of these features.

The second query (query 2 = Q2, Figure 3) was built on the basis of the features of the docked substrate and spatially constrained by the surrounding binding cavity of MGL. Hydrophobic centers were set at carbons C6 and C10 of **1** (tolerance 1.0 Å; see Figure 1 for numbering the carbon atoms of **1**). Partial match was used so that at least one hydrophobic center should match with the hit molecules. Both hydroxyl groups of **1** were defined as donor and acceptor atoms and the ether and carbonyl oxygens as acceptor atoms (tolerance 0.3 Å). A partial match was employed so that at least one and at most five of these features would match with the hit molecules. A similar surface volume constraint to that in the

first query was used also for this query. Q1 was used to search through the LeadQuest database⁴⁸ (April 2003) and Q2 for both the LeadQuest and Maybridge²⁹ databases. Flex Search method was used in all cases, and a maximum molecular weight of 450 g/mol was set as a hit filter. The search process with Q1 had to be discontinued as the processing of the task was terminated. However, all 97 hit molecules found through this search were saved for later analysis. Both searches with Q2 were successfully completed.

Filtering the Hit Molecules for Biological Evaluation. The hit molecules obtained with both queries as well as **7** from the CB2 ligand search²¹ were docked at the MGL model with GOLD v. 2.1. The hits from the Q1 search were docked into a cavity ($r = 18 \text{ \AA}$) surrounding the hydroxyl oxygen of Ser122, allowing maximally 15 different conformations for each ligand, whereas the hits from Q2 searches were docked into the same but a slightly smaller cavity ($r = 15 \text{ \AA}$), allowing the program to produce only 10 conformations for each ligand. The resulting docking conformations were scored with CScore, and the G score⁴⁹ function of CScore was used to rank the ligand conformations. The rationale for using the G score function in the present study was based on our previous results of docking known nonselective MGL/FAAH inhibitors (MAFP; HDSF; phenylmethylsulfonyl fluoride, PMSF; arachidonyl trifluoromethyl ketone, ATRFMK; bromoenol lactone; URB597, and **7**) into the MGL model. In that preliminary docking study, the G score function ranked the most potent inhibitor MAFP as the best (data not shown). The 30 best-ranked molecules from both LeadQuest and Maybridge databases (altogether 60) were chosen for further analysis. Finally, 23 compounds from LeadQuest and 28 from Maybridge were chosen to be ordered and tested for their biological activity.

BRUTUS Database Searches. In addition to using the UNITY module for the database searches, also the fast grid-based algorithm BRUTUS²⁴ was utilized. Compounds **1** and **7**, both docked at MGL, were used as template molecules on which the database molecules were superimposed according to the electrostatic and steric molecular fields. Compound **7** had been previously found through the virtual screening of CB2 ligands²¹ and had been discovered to inhibit MGL. For compound **1** we chose the same conformation as used in the UNITY queries and for compound **7** its best-ranked conformation (rank order according to the G Score function of CScore; see above). With both templates, we searched through the local Maybridge database in which we had several conformations of each compound.²⁴ MMFF94 charges^{50–56} were applied for both the template and the database compounds. The compound alignments that had field similarity scores smaller than 0.6 for vdW, 0.3 for ESP – vdW, and 0.5 for ESP + vdW were filtered out during the search (see ref 24 for a detailed explanation of these field combinations). The same SOM (self-organizing map) procedure as utilized in a previously reported study by Tervo et al.²⁴ was used to classify the numerical characterization of the aligned field data (SOM size 32 neurons \times 32 neurons). Three molecules with great similarity to **1** and eight with great similarity to **7** were ordered to be tested for their biological activity.

Compounds. Compound **1** was purchased from Cayman Chemical (Ann Arbor, MI). Radiolabeled *N*-arachidonylethanolamide [ethanolamine 1-³H] ([³H]AEA, 60 Ci mmol⁻¹) was obtained from American Radiolabeled Chemicals (St. Louis, MO). Bovine serum albumin (BSA, essentially fatty acid free) was purchased from Sigma (St. Louis, MO). Virtual screening hit molecules were obtained from Maybridge Chemical Company Ltd (Trevillet, Cornwall, England) and Tripos Associated Inc. (LeadQuest Compound Library, St. Louis, MO).

Animals and Preparation of Rat Brain Homogenate. Eight-week-old male Wistar rats were used in these studies. All animal experiments were approved by the local ethics committee. The animals lived in a 12-h light/12-h dark cycle (lights on at 0700 h) with water and food available ad libitum.

The rats were decapitated, and whole brains minus cerebellum were dissected and homogenized in one volume (v/w) of ice-cold 0.1 M potassium phosphate buffer (pH 7.4) with a Potter-Elvehjem homogenizer (Heidolph). The homogenate was centrifuged at

10 000g for 20 min at 4 °C, and the resulting supernatant was used as a source of FAAH activity. The protein concentration of the supernatant (7.2 mg/mL) was determined by the method of Bradford with BSA as a standard (Bradford, 1976). Aliquots of the supernatant were stored at –80 °C until use.

Animals and Preparation of Rat Cerebellar Membranes. Four-week-old male Wistar rats were used in these studies. All animal experiments were approved by the local ethics committee. The animals lived in a 12-h light/12-h dark cycle (lights on at 0700 h), with water and food available ad libitum. The rats were decapitated, 8 h after lights on (1500 h), whole brains were removed, dipped in isopentane on dry ice and stored at –80 °C. Membranes were prepared as previously described.^{57–59}

Briefly, cerebella (minus brain stem) from eight animals were weighed and homogenized in nine volumes of ice-cold 0.32 M sucrose with a glass Teflon homogenizer. The crude homogenate was centrifuged at low speed (1000g for 10 min at 4 °C), and the pellet was discharged. The supernatant was centrifuged at high speed (100 000g for 10 min at 4 °C). The pellet was resuspended in ice-cold deionized water and washed twice, repeating the high-speed centrifugation. Finally, membranes were resuspended in 50 mM Tris-HCl, pH 7.4 with 1 mM EDTA and aliquoted for storage at –80 °C. The protein concentration of the final preparation, measured by the Bradford method,⁶⁰ was 11 mg mL⁻¹.

In Vitro Assay for FAAH Activity. All purchased compounds were tested for their potential FAAH inhibitory activity in the assay described for the first time in this paper. The endpoint enzymatic assay was developed to quantify FAAH activity with tritium labeled arachidonylethanolamide [ethanolamine 1-³H]. The assay buffer was 0.1 M potassium phosphate (pH 7.4) used, and test compounds were dissolved in DMSO (the final DMSO concentration was max 5% v/v). The incubations were performed in the presence of 0.5% (w/v) BSA (essentially fatty acid free). Test compounds were preincubated with rat brain homogenate protein (18 μ g) for 10 min at 37 °C (60 μ L). At the 10 min time point, arachidonylethanolamide was added so that its final concentration was 2 μ M (containing $50 \times 10^{-3} \mu$ Ci of 60 Ci/mmol [³H]AEA), and the final incubation volume was 100 μ L. The incubations proceeded for 10 min at 37 °C. Ethyl acetate (400 μ L) was added at the 20 min time point to stop the enzymatic reaction. Additionally, 100 μ L of unlabeled ethanolamine (1 mM) was added as a ‘carrier’ for radioactive ethanolamine. Samples were centrifuged at 16 000g for 4 min at RT, and aliquots (100 μ L) from the aqueous phase containing [ethanolamine 1-³H] were measured for radioactivity by liquid scintillation counting (Wallac 1450 MicroBeta; Wallac Oy, Finland). Under these conditions, the rate of [ethanolamine 1-³H] formation was linear with respect to the protein concentration up to 30 μ g as well as up to the 20 min incubation time (data not shown). In response to increasing concentration of the substrate [³H]AEA, the enzyme activity in rat brain homogenate showed a typical saturation curve of the Michaelis–Menten type with a K_m value of $5.9 \pm 0.6 \mu$ M and a V_{max} value of $1.03 \pm 0.05 \text{ nmol}^{-1} \text{ min}^{-1} \text{ mg protein}$ (mean \pm SEM; $n = 2$).

In Vitro Assay for MGL Activity. The assay for MGL has been described previously.¹⁸ Briefly, experiments were carried out with preincubations (80 μ L, 30 min at 25 °C) containing 10 μ g of membrane protein, 44 mM Tris-HCl (pH 7.4), 0.9 mM EDTA, 0.5% (wt/vol) BSA, and 1.25% (vol/vol) DMSO as a solvent for inhibitors. The preincubated membranes were kept at 0 °C just prior to the experiments. The incubations (90 min at 25 °C) were initiated by adding 40 μ L of preincubated membrane cocktail, in a final volume of 400 μ L. The final volume contained 5 μ g of membrane protein, 54 mM Tris-HCl (pH 7.4), 1.1 mM EDTA, 100 mM NaCl, 5 mM MgCl₂, 0.5% (wt/vol) BSA, and 50 μ M of **1**. At time-points of 0 and 90 min, 100 μ L-samples were removed from the incubation, acetonitrile (200 μ L) was added to stop the enzymatic reaction, and the pH of the samples was simultaneously decreased to 3.0 with phosphoric acid (added to acetonitrile) to stabilize compound **1** against acyl migration to 1(3)-AG. Samples were centrifuged at 23 700g for 4 min at RT prior to HPLC analysis of the supernatant.

HPLC Method. The analytical HPLC was performed as previously described.²⁰ Briefly, the analytical HPLC system consisted of a Merck Hitachi (Hitachi Ltd., Tokyo, Japan) L-7100 pump, D-7000 interface module, L-7455 diode-array UV detector (190–800 nm, set at 211 nm), and L-7250 programmable autosampler. The separations were accomplished on a Zorbax SB-C18 end-capped reversed-phase precolumn (4.6 × 12.5 mm, 5 μm) and column (4.6 × 150 mm, 5 μm) (Agilent Technologies Inc., Wilmington, DE). The injection volume was 50 μL. A mobile phase mixture of 28% phosphate buffer (30 mM, pH 3.0) in acetonitrile was used at a flow rate of 2.0 mL min⁻¹. Retention times were 5.8 min for **1**, 6.3 min for 1(3)-AG, and 10.2 min for arachidonic acid. The relative concentrations of **1**, 1(3)-AG, and arachidonic acid were determined by the corresponding peak areas. This was justified by the equivalence of response factors for the studied compounds and was supported by the observation that the sum of the peak areas was constant throughout the experiments.

Data Analyses. The results from the enzyme inhibition experiments are presented as mean ± 95% confidence intervals (CI) of at least three independent experiments performed in duplicate. Data analyses for the dose–response curves were calculated as nonlinear regressions using GraphPad Prism 4.0 for Windows.

Docking of the Discovered FAAH Inhibitors at FAAH. The found FAAH inhibitors were docked at the putative binding site of FAAH by the GOLD program (v. 3.0). The hydroxyl oxygen of the catalytic Ser241 was used as a center atom for defining the docking cavity (cavity radius = 25 Å) using the automatic settings with a 200% search efficiency. The maximum number of dockings per compound was set to ten. The GOLD Score⁴⁹ was used as a fitness function. All other parameters were kept as set by default. All docking conformations were then relaxed and ranked with the CScore, and the conformations with the best scores were checked visually.

Acknowledgment. The authors thank the National Technology Agency of Finland, the Academy of Finland (grant #107300), and CSC – Scientific Computing Ltd for computational resources. We also thank Toni Rönkkö (M. Sc.) and Ms. Helly Rissanen for their technical assistance.

Supporting Information Available: Modeling alignment for the MGL and chloroperoxidase L sequences; molecular dynamics parameters and simulation constraints; total energy, rmsd, and secondary structure plots for the MD simulation; PROCHECK summaries. This material is available free of charge via the Internet at <http://pubs.acs.org>.

References

- Devane, W. A.; Hanus, L.; Breuer, A.; Pertwee, R. G.; Stevenson, L. A.; Griffin, G.; Gibson, D.; Mandelbaum, A.; Etinger, A.; Mechoulam, R. Isolation and structure of a brain constituent that binds to the cannabinoid receptor. *Science* **1992**, *258*, 1946–1949.
- Mechoulam, R.; Ben-Shabat, S.; Hanus, L.; Ligumsky, M.; Kaminski, N. E.; Schatz, A. R.; Gopher, A.; Almog, S.; Martin, B. R.; Compton, D. R.; et al. Identification of an endogenous 2-monoglyceride, present in canine gut, that binds to cannabinoid receptors. *Biochem. Pharmacol.* **1995**, *50*, 83–90.
- Sugiura, T.; Kondo, S.; Sukagawa, A.; Nakane, S.; Shinoda, A.; Itoh, K.; Yamashita, A.; Waku, K. 2-Arachidonoylglycerol: a possible endogenous cannabinoid receptor ligand in brain. *Biochem. Biophys. Res. Commun.* **1995**, *215*, 89–97.
- Di Marzo, V.; Fontana, A.; Cadas, H.; Schinelli, S.; Cimino, G.; Schwartz, J. C.; Piomelli, D. Formation and inactivation of endogenous cannabinoid anandamide in central neurons. *Nature* **1994**, *372*, 686–691.
- Schmid, P. C.; Zuzarte-Augustin, M. L.; Schmid, H. H. Properties of rat liver N-acyl ethanolamine amidohydrolase. *J. Biol. Chem.* **1985**, *260*, 14145–14149.
- Deutsch, D. G.; Chin, S. A. Enzymatic synthesis and degradation of anandamide, a cannabinoid receptor agonist. *Biochem. Pharmacol.* **1993**, *46*, 791–796.
- Cravatt, B. F.; Giang, D. K.; Mayfield, S. P.; Boger, D. L.; Lerner, R. A.; Gilula, N. B. Molecular characterization of an enzyme that degrades neuromodulatory fatty-acid amides. *Nature* **1996**, *384*, 83–87.
- Dinh, T. P.; Kathuria, S.; Piomelli, D. RNA interference suggests a primary role for monoacylglycerol lipase in the degradation of the endocannabinoid 2-arachidonoylglycerol. *Mol. Pharmacol.* **2004**, *66*, 1260–1264.
- Di Marzo, V.; Bisogno, T.; Sugiura, T.; Melck, D.; De Petrocellis, L. The novel endogenous cannabinoid 2-arachidonoylglycerol is inactivated by neuronal- and basophil-like cells: connections with anandamide. *Biochem. J.* **1998**, *331* (Pt 1), 15–19.
- Tornqvist, H.; Belfrage, P. Purification and some properties of a monoacylglycerol-hydrolyzing enzyme of rat adipose tissue. *J. Biol. Chem.* **1976**, *251*, 813–819.
- Jayamanne, A.; Greenwood, R.; Mitchell, V. A.; Aslan, S.; Piomelli, D.; Vaughan, C. W. Actions of the FAAH inhibitor URB597 in neuropathic and inflammatory chronic pain models. *Br. J. Pharmacol.* **2005**.
- Kathuria, S.; Gaetani, S.; Fegley, D.; Valino, F.; Duranti, A.; Tontini, A.; Mor, M.; Tarzia, G.; La Rana, G.; Calignano, A.; Giustino, A.; Tattoli, M.; Palmery, M.; Cuomo, V.; Piomelli, D. Modulation of anxiety through blockade of anandamide hydrolysis. *Nat. Med.* **2003**, *9*, 76–81.
- Deutsch, D. G.; Omeir, R.; Arreaza, G.; Salehani, D.; Prestwich, G. D.; Huang, Z.; Howlett, A. Methyl arachidonoyl fluorophosphonate: a potent irreversible inhibitor of anandamide amidase. *Biochem. Pharmacol.* **1997**, *53*, 255–260.
- Deutsch, D. G.; Lin, S.; Hill, W. A.; Morse, K. L.; Salehani, D.; Arreaza, G.; Omeir, R. L.; Makriyannis, A. Fatty acid sulfonyl fluorides inhibit anandamide metabolism and bind to the cannabinoid receptor. *Biochem. Biophys. Res. Commun.* **1997**, *231*, 217–221.
- Boger, D. L.; Sato, H.; Lerner, A. E.; Hedrick, M. P.; Fecik, R. A.; Miyauchi, H.; Wilkie, G. D.; Austin, B. J.; Patricelli, M. P.; Cravatt, B. F. Exceptionally potent inhibitors of fatty acid amide hydrolase: the enzyme responsible for degradation of endogenous oleamide and anandamide. *Proc. Natl. Acad. Sci. U.S.A.* **2000**, *97*, 5044–5049.
- Boger, D. L.; Miyauchi, H.; Du, W.; Hardouin, C.; Fecik, R. A.; Cheng, H.; Hwang, I.; Hedrick, M. P.; Leung, D.; Acevedo, O.; Guimaraes, C. R.; Jorgensen, W. L.; Cravatt, B. F. Discovery of a potent, selective, and efficacious class of reversible alpha-ketoheterocycle inhibitors of fatty acid amide hydrolase effective as analgesics. *J. Med. Chem.* **2005**, *48*, 1849–1856.
- Makara, J. K.; Mor, M.; Fegley, D.; Szabo, S. I.; Kathuria, S.; Astarita, G.; Duranti, A.; Tontini, A.; Tarzia, G.; Rivara, S.; Freund, T. F.; Piomelli, D. Selective inhibition of 2-AG hydrolysis enhances endocannabinoid signaling in hippocampus. *Nat. Neurosci.* **2005**, *8*, 1139–1141.
- Saario, S. M.; Salo, O. M.; Nevalainen, T.; Poso, A.; Laitinen, J. T.; Jarvinen, T.; Niemi, R. Characterization of the sulfhydryl-sensitive site in the enzyme responsible for hydrolysis of 2-arachidonoylglycerol in rat cerebellar membranes. *Chem. Biol.* **2005**, *12*, 649–656.
- Dinh, T. P.; Carpenter, D.; Leslie, F. M.; Freund, T. F.; Katona, I.; Sensi, S. L.; Kathuria, S.; Piomelli, D. Brain monoglyceride lipase participating in endocannabinoid inactivation. *Proc. Natl. Acad. Sci. U.S.A.* **2002**, *99*, 10819–10824.
- Saario, S. M.; Savinainen, J. R.; Laitinen, J. T.; Jarvinen, T.; Niemi, R. Monoglyceride lipase-like enzymatic activity is responsible for hydrolysis of 2-arachidonoylglycerol in rat cerebellar membranes. *Biochem. Pharmacol.* **2004**, *67*, 1381–1387.
- Salo, O. M.; Raitio, K. H.; Savinainen, J. R.; Nevalainen, T.; Lahtela-Kakkonen, M.; Laitinen, J. T.; Jarvinen, T.; Poso, A. Virtual screening of novel CB2 ligands using a comparative model of the human cannabinoid CB2 receptor. *J. Med. Chem.* **2005**, *48*, 7166–7171.
- Laskowski, R. A.; MacArthur, M. W.; Moss, D. S.; Thornton, J. M. PROCHECK: a program to check the stereochemical quality of protein structures. *J. Appl. Crystallogr.* **1993**, *26*, 283–291.
- Bifulco, M.; Laezza, C.; Valenti, M.; Ligresti, A.; Portella, G.; Di Marzo, V. A new strategy to block tumor growth by inhibiting endocannabinoid inactivation. *FASEB J.* **2004**, *18*, 1606–1608.
- Tervo, A. J.; Rönkkö, T.; Nyrönen, T. H.; Poso, A. BRUTUS: optimization of a grid-based similarity function for rigid-body molecular superposition. I. Alignment and virtual screening applications. *J. Med. Chem.* **2005**, *48*, 4076–4086.
- Rönkkö, T. P.; Tervo, A. J.; Parkkinen, J.; Poso, A. BRUTUS: Optimization of a grid-based similarity function for rigid-body molecular superposition. II. Description and characterization. *J. Comput.-Aided Mol. Des.* **2006**, in press.
- LeadQuest Compound Library, Tripos Associates, Inc.: St. Louis, MO. <http://leadquest.tripos.com/>.
- Brickmann, J.; Goetze, T.; Heiden, W.; Moeckel, G.; Reiling, S.; Vollhardt, H.; Zachmann, C.-D. Interactive Visualization of Molecular Scenarios with MOLCAD/SYBYL. In *Data Visualization in Molecular Science – Tools for Insight and Innovation*, Bowie, J. E., Ed.; Addison-Wesley Publishing Company Inc.: Reading, MA, 1995; pp 83–97.

- (28) SYBYL v. 7.1, Tripos Associates, Inc.: St. Louis, MO. <http://www.tripos.com/>.
- (29) Giuffrida, A.; Parsons, L. H.; Kerr, T. M.; Rodriguez de Fonseca, F.; Navarro, M.; Piomelli, D. Dopamine activation of endogenous cannabinoid signaling in dorsal striatum. *Nat. Neurosci.* **1999**, *2*, 358–363.
- (30) Mentlein, R.; Suttorp, M.; Heymann, E. Specificity of purified monoacylglycerol lipase, palmitoyl-CoA hydrolase, palmitoyl-carnitine hydrolase, and nonspecific carboxylesterase from rat liver microsomes. *Arch. Biochem. Biophys.* **1984**, *228*, 230–246.
- (31) Tornqvist, H.; Belfrage, P. Purification and some properties of a monoacylglycerol-hydrolyzing enzyme of rat adipose tissue. *J. Biol. Chem.* **1976**, *251*, 813–819.
- (32) Bracey, M. H.; Hanson, M. A.; Masuda, K. R.; Stevens, R. C.; Cravatt, B. F. Structural adaptations in a membrane enzyme that terminates endocannabinoid signaling. *Science* **2002**, *298*, 1793–1796.
- (33) Boeckmann, B.; Bairoch, A.; Apweiler, R.; Blatter, M. C.; Estreicher, A.; Gasteiger, E.; Martin, M. J.; Michoud, K.; O'Donovan, C.; Phan, I.; Pilbout, S.; Schneider, M. The SWISS-PROT protein knowledgebase and its supplement TrEMBL in 2003. *Nucleic Acids Res.* **2003**, *31*, 365–370.
- (34) Hofmann, B.; Tolzer, S.; Pelletier, I.; Altenbuchner, J.; van Pee, K. H.; Hecht, H. J. Structural investigation of the cofactor-free chloroperoxidases. *J. Mol. Biol.* **1998**, *279*, 889–900.
- (35) Berman, H. M.; Battistuz, T.; Bhat, T. N.; Bluhm, W. F.; Bourne, P. E.; Burkhardt, K.; Feng, Z.; Gilliland, G. L.; Iype, L.; Jain, S.; Fagan, P.; Marvin, J.; Padilla, D.; Ravichandran, V.; Schneider, B.; Thanki, N.; Weissig, H.; Westbrook, J. D.; Zardecki, C. The Protein Data Bank. *Acta Crystallogr. D. Biol. Crystallogr.* **2002**, *58*, 899–907.
- (36) *InsightII v. 2000*, Accelrys, Inc.: San Diego, CA. <http://www.accelrys.com/>.
- (37) SYBYL v. 6.9, Tripos Associates, Inc.: St. Louis, MO. <http://www.tripos.com/>.
- (38) Weiner, S. J.; Kollman, P. A.; Case, D. A.; Singh, U. C.; Ghio, C.; Alagona, G.; Profeta, S.; Weiner, J. P. A new force field for molecular mechanical simulation of nucleic acids and proteins. *J. Am. Chem. Soc.* **1984**, *106*, 765–784.
- (39) Weiner, S. J.; Kollman, P. A.; Nguyen, D. T.; Case, D. A. An all atom force field for simulations of proteins and nucleic acid. *J. Comput. Chem.* **1986**, *11*, 431–439.
- (40) Tsuboi, K.; Sun, Y. X.; Okamoto, Y.; Araki, N.; Tonai, T.; Ueda, N. Molecular characterization of N-acyl ethanolamine-hydrolyzing acid amidase, a novel member of the cholesteryl glycerol hydrolase family with structural and functional similarity to acid ceramidase. *J. Biol. Chem.* **2005**, *280*, 11082–11092.
- (41) Lindahl, E.; Hess, B.; van der Spoel, D. GROMACS 3.0: A package for molecular simulation and trajectory analysis. *J. Mol. Model.* **2001**, *7*, 306–317.
- (42) Jorgensen, W. L.; Chandrasekhar, J.; Madura, J. D.; Impey, R. W.; Klein, M. L. Comparison of simple potential functions for simulating liquid water. *J. Chem. Phys.* **1983**, *79*, 926–935.
- (43) van Gunsteren, W. F.; Berendsen, H. J. C. *Gromos-87 manual*. Biomos BV Nijenborgh 4, 9747 AG Groningen, The Netherlands: 1987.
- (44) Essman, U.; Perela, L.; Berkowitz, M. L.; Darden, T.; Lee, H.; Pedersen, L. G. A smooth particle mesh Ewald method. *J. Chem. Phys.* **1995**, *103*, 8577–8592.
- (45) Berendsen, H. J. C.; Postma, J. P. M.; DiNola, A.; Haak, J. R. Molecular dynamics with coupling to an external bath. *J. Chem. Phys.* **1984**, *81*, 3684–3690.
- (46) *GOLD v. 2.0*, Cambridge Crystallographic Data Centre: Cambridge, U.K. http://www.ccdc.cam.ac.uk/products/life_sciences/gold/.
- (47) *CScore*, Tripos Associates, Inc.: St. Louis, MO. <http://www.tripos.com/sciTech/inSilicoDisc/virtualScreening/cscore.html#references>.
- (48) Ligresti, A.; Bisogno, T.; Matias, I.; De Petrocellis, L.; Cascio, M. G.; Cosenza, V.; D'Argenio, G.; Scaglione, G.; Bifulco, M.; Sorrentini, I.; Di Marzo, V. Possible endocannabinoid control of colorectal cancer growth. *Gastroenterology* **2003**, *125*, 677–687.
- (49) Jones, G.; Willett, P.; Glen, R. C.; Leach, A. R.; Taylor, R. Development and validation of a genetic algorithm for flexible docking. *J. Mol. Biol.* **1997**, *267*, 727–748.
- (50) Halgren, T. A. Merck molecular force field. I. Basis, form, scope, parameterization, and performance of MMFF94. *J. Comput. Chem.* **1996**, *17*, 490–519.
- (51) Halgren, T. A. Merck molecular force field. II. MMFF94 van der Waals and electrostatic parameters for intermolecular interactions. *J. Comput. Chem.* **1996**, *17*, 520–552.
- (52) Halgren, T. A. Merck molecular force field. III. Molecular geometries and vibrational frequencies for MMFF94. *J. Comput. Chem.* **1996**, *17*, 553–586.
- (53) Halgren, T. A.; Nachbar, R. B. Merck molecular force field. IV. conformational energies and geometries for MMFF94. *J. Comput. Chem.* **1996**, *17*, 587–615.
- (54) Halgren, T. A. Merck molecular force field. V. Extension of MMFF94 using experimental data, additional computational data, and empirical rules. *J. Comput. Chem.* **1996**, *17*, 616–641.
- (55) Halgren, T. A. MMFF VI. MMFF94s Option for Energy Minimization Studies. *J. Comput. Chem.* **1999**, *20*, 720–729.
- (56) Halgren, T. A. MMFF VII. Characterization of MMFF94, MMFF94s, and other widely available force fields for conformational energies and for intermolecular-interaction energies and geometries. *J. Comput. Chem.* **1999**, *20*, 730–748.
- (57) Lorenzen, A.; Fuss, M.; Vogt, H.; Schwabe, U. Measurement of guanine nucleotide-binding protein activation by A1 adenosine receptor agonists in bovine brain membranes: stimulation of guanosine-5'-O-(3-[35S]thio)triphosphate binding. *Mol. Pharmacol.* **1993**, *44*, 115–123.
- (58) Kurkinen, K. M.; Koistinaho, J.; Laitinen, J. T. [Gamma-35S]GTP autoradiography allows region-specific detection of muscarinic receptor-dependent G-protein activation in the chick optic tectum. *Brain Res.* **1997**, *769*, 21–28.
- (59) Savinainen, J. R.; Jarvinen, T.; Laine, K.; Laitinen, J. T. Despite substantial degradation, 2-arachidonoylglycerol is a potent full efficacy agonist mediating CB(1) receptor-dependent G-protein activation in rat cerebellar membranes. *Br. J. Pharmacol.* **2001**, *134*, 664–672.
- (60) Bradford, M. M. A rapid and sensitive method for the quantitation of microgram quantities of protein utilizing the principle of protein-dye binding. *Anal. Biochem.* **1976**, *72*, 248–254.

JM060394Q